

Article

Effect of Low Magnetic Field on Biomimetic Deposition of Hydroxyapatite on Titanium and BIOLINE Stainless Steel

Rafael Uribe ^{1,*} , Andrea Uvillús ¹, Omar Bonilla ¹, Luis Lascano ²  and Gema González ^{3,4,*} 

¹ Departamento de Ingeniería Química, Escuela Politécnica Nacional, P.O. Box 17-01-2759, Quito 170525, Ecuador; andrea.uvillus@epn.edu.ec (A.U.); omar.bonilla@epn.edu.ec (O.B.)

² Departamento de Física, Escuela Politécnica Nacional, P.O. Box 17-01-2759, Quito 170525, Ecuador; luis.lascano@epn.edu.ec

³ School of Physical Sciences and Nanotechnology, Yachay Tech University, Urcuqui 100650, Ecuador

⁴ Centro de Ingeniería Materiales y Nanotecnología, Instituto Venezolano de Investigaciones Científicas, Caracas 1020-A, Venezuela

* Correspondence: rafael.uribe@epn.edu.ec (R.U.); ggonzalez@yachaytech.edu.ec (G.G.); Tel.: +593-959651664 (R.U.)

Abstract: In this work, we evaluated the effect of a low magnetic field on the deposition of hydroxyapatite (HAp) on different metallic substrates. The substrates studied were titanium and BIOLINE stainless steel SS316LVM with and without Ta and TaN/Ta coatings. Before deposition, the uncoated Ti and SS316LVM substrates were treated with alkali to improve the adhesion of the films prompted to be formed. Next, all substrates (coated and uncoated) were immersed in stimulated body fluid (SBF) at physiological conditions of 37 °C, pH = 7.4, in the presence of magnetic fields from 0.15 T and 0.22 T for 7, 10, and 14 days. The formed films were characterized using SEM, FTIR, and the contact angle. Ti and SS316LVM substrates presented Ca/P relations closer to the stoichiometric HAp. It was demonstrated that in both coatings, Ta and Ta/N, an increase of the bioactivity was obtained. Additionally, our results showed that the application of magnetic fields has a significant effect on the increment in the mass:area ratio of HAp. Finally, the contact angle values were lower than 90°, showing an increase in hydrophilicity with respect to the metallic substrates.

Keywords: hydroxyapatite; biomaterials; titanium-biocompatible substrates; BIOLINE stainless steel SS316LVM



Citation: Uribe, R.; Uvillús, A.; Bonilla, O.; Lascano, L.; González, G. Effect of Low Magnetic Field on Biomimetic Deposition of Hydroxyapatite on Titanium and BIOLINE Stainless Steel. *Coatings* **2021**, *11*, 1484. <https://doi.org/10.3390/coatings11121484>

Academic Editors: Patrick Tang, Siah Ying and Lech Pawlowski

Received: 9 September 2021

Accepted: 23 November 2021

Published: 2 December 2021

Publisher's Note: MDPI stays neutral with regard to jurisdictional claims in published maps and institutional affiliations.



Copyright: © 2021 by the authors. Licensee MDPI, Basel, Switzerland. This article is an open access article distributed under the terms and conditions of the Creative Commons Attribution (CC BY) license (<https://creativecommons.org/licenses/by/4.0/>).

1. Introduction

Every year, more than 2.2 million people worldwide require prosthetics or bone grafting due to accidents, trauma, or degenerative diseases, which generates an increasing demand for new technologies for implant fabrication [1]. Nowadays, metallic orthopedic prosthetic implants are made principally of stainless steel (SS), titanium (Ti), and titanium-magnesium alloys, due to their mechanical resistance and inert characteristics. Nevertheless, the lack of interaction between the metallic implants and bone tissue avoids the integration of the first with the surrounding hard tissue, with long-term consequences such as anomalies related to foreign-body rejection and corrosion [2]. For example, titanium $\alpha + \beta$ type Ti-6Al-4V ELI has been used in orthopedic applications because it has biocompatibility and a relatively low modulus of elasticity [3]. Titanium also has excellent physical and mechanical properties, such as tensile and fatigue strength, low density, and good corrosion resistance; these are the advantages of titanium as an implant material [4]. Nevertheless, titanium presents a low bioactive surface with low osseointegration [5].

To avoid these complications, implant protection using different biocompatible coatings and hydroxyapatite (HAp) deposition on different substrates is one of the most widely used methods in both bone and dental implants, due to the excellent biocompatibility, bioactivity, and bone integration of HAp [5–7].

The most important methods used to form HAp coatings on metallic substrates are sputtering, plasma spraying, and pulsed laser deposition, among others [8–10]. Al-Amin et al. [9] present a comparative analysis of machined surface properties using existing deposition methods with HAp. The dominance of process factors over performance is discussed thoroughly. The biomimetic method developed by Kokubo et al. [11] is also widely used. This approach consists in the immersion of a material in simulated body fluid (SBF) with a composition that imitates the inorganic characteristics of blood plasma and mimics the physiological conditions of the human body during the biomineralization process. One of the limitations of this method is the long time required to form a uniform film of HAp, spanning 30–45 days or even months [12,13]. Several alternatives have been developed to diminish the time required to form an HAp film on different substrates, such as increasing the concentration of the simulated body fluid [12]. For instance, Pecheva et al. [14] performed a study on AISI 316 steel using SBF with a concentration of calcium and phosphorus ions 1.5 times higher than the one proposed by Kokubo et al. [11], obtaining nucleation of HAp on the steel surface after 5 days. In contrast, Thirugnanam et al. [8] carried out chemical treatments of oxidation and precalcination on titanium surfaces, achieving a reasonable amount of HAp deposits when compared to chemically untreated samples. Their results showed that for the chemically treated samples, a Ca/P ratio of 1.6 was obtained, which is close to the non-stoichiometric ratio of HAp. It was shown that titanium ions originated from the corrosion reaction in body fluids and caused negative immune reactions or skin allergies immediately or shortly after implant fixation [15]. Therefore, it is crucial to design a coating that will make titanium and stainless steel surfaces more bioactive/osseointegrative and, at the same time, more corrosion resistant during long-term exposure to oral cavity fluids [16].

In contrast, tantalum and tantalum nitride have also shown excellent biocompatibility and effective integration to bone [17–20]. The development of Ta and TaN with bone-bonding ability is of interest because of their attractive features, such as high fracture toughness, high workability, and clinical usage [20]. Apatite nucleation on the surface of the tantalum metal progresses via a simple chemical treatment that rapidly forms functional groups effective for the apatite nucleation on a material surface; thus, Ta has high potential for design of novel biomaterials with bone-bonding ability. Additionally, the coating of stainless steel with TaN/Ta would improve the corrosion, wear resistance, and biocompatibility of the base metal.

It is well known that HAp is the most stable thermodynamic phase among calcium phosphates, with a Ca/P ratio of 1.67. Nevertheless, several studies have shown that HAp is preceded by several precursor phases, such as amorphous calcium phosphate (ACP), dicalcium phosphate dehydrated (DCPD), octacalcium phosphate (OCP), and calcium-deficient HAp (CDHA), which depends on the temperature, pH, and inhibitors that may be present in the environment [21–23]. The method to obtain HAp as a bone substitute should offer specific characteristics, such as high purity, performance, and low cost [21–24].

There are few reports studying the effect of magnetic fields on the deposition of HAp [23–27]. Most of the works deal with the effect of the magnetic field in the crystallization, orientation, and morphology of HAp crystals. The magnetic field effects have been mainly attributed to the magnetic pair induced by the anisotropy of the magnetic susceptibility [23,25]. Sundaram et al. [26] showed that in the presence of a magnetic field of 0.1 T on SBF gel, the formation of the HAp phase is favored. In contrast, Siddharthan et al. [27] observed that the presence of a static magnetic field of 0.1 T has an influence on the formation of HAp on titanium substrates, obtaining denser coatings when compared to non-irradiated titanium.

This present evaluates the effect of magnetic fields of 0.1–0.3 T on titanium and BIO-LINE SS316LVM substrates with and without Ta, Ta/N, and Ta/TaN coatings, immersed in SBF, and evaluates the deposition time and morphology of HAp on these substrates. To the best of our knowledge, there are no reports on the formation of HAp in the presence of magnetic fields on these metallic substrates.

2. Materials and Methods

In this work, six different types of substrates were used: uncoated titanium (Ti, 12 mm diameter, 99.99% purity, from Sigma-Aldrich), stainless steel (SS)-type BIOLINE SS316LVM (10 mm diameter) from Sandvik, tantalum-coated titanium (Ta/Ti), tantalum-coated stainless steel (Ta/SS), tantalum- and tantalum-nitride-coated titanium (Ta/TaN/Ti), and tantalum- and tantalum-nitride-coated stainless steel (Ta/TaN/SS). The Ta, TaN, and Ta/Ta/N coatings were prepared via cathodic deposition (sputtering) in RF ALCATEL DION 300 sputtering equipment (Grenoble, France), with a cathode of 99.96% Ta [28]. The bare metallic substrates were superficially treated through metallographic preparation until a mirror-finished surface was accomplished, following the ASTM E03-1:2010 norm [29]. Next, the substrates were introduced in an ultrasound bath for 5 min and then washed with alcohol and deionized water. Afterward, the uncoated substrate surface was etched with acid (HCl and H₂SO₄) and alkaline (10 M NaOH) treatment at 60 °C for 24 h [8]. In the titanium substrates and Ta coatings, a thin film of sodium titanate or tantalum titanate was obtained by the reaction $\text{Ti} + 2\text{NaOH} + \text{H}_2\text{O} \rightarrow \text{Na}_2\text{TiO}_3 + 2\text{H}_2$; a similar reaction was obtained with Ta substrates.

2.1. Characterization of Metallic Substrates

The metallic substrates were characterized using scanning electron microscopy (SEM) using FEI Inspec F50 equipment (Eindhoven, The Netherlands) elemental analysis (EDS), X-ray diffraction (XRD) with BRUKER AXS equipment (Wisconsin, USA) with CuK α radiation operated at 45 kV and 30 mA, and surface XRD at 45 kV and 20 mA with an offset of 7°. In addition, hydrophilicity trials were carried out on the different substrates via measurement of the contact angle: a water droplet was placed over the different substrates using a 1 μ L micropipette; this was performed in a chamber with controlled temperature and pressure [30]. A picture of the drop on the substrate was taken using a Thorlabs camera (New Jersey, NJ, USA), model DC1240C, TYPE CMOS, 1280 \times 1024 pixels. Each drop covering was calculated from the surface area covered by the drop once on the substrate. The area covered by the drop over the different substrates was calculated assuming that the drop covers a circular area, and from the diameter of the deposited drop the covered area was calculated. Table 1 shows the different areas covered by each drop on the different substrates. To eliminate the relative error and obtain an average value, five repetitions of the contact angle were carried out at different times on the same substrate.

Table 1. Area covered by a drop of water on the different substrates.

Substrate	Bare Substrate	Diameter	Area	After Deposition of HAp	Diameter	Area
	Angle (°)	(mm)	(mm ²)	Angle (°)	(mm)	(mm ²)
Ti	67.08 \pm 0.63	3.1	7.55	44.15 \pm 0.99	6.01	28.37
Ta/Ti	48.52 \pm 0.91	5.42	23.07	44.88 \pm 0.70	5.92	27.53
Ta/TaN/Ti	46.22 \pm 0.66	4.33	14.73	35.80 \pm 0.63	6.18	30.00
SS316SVM	46.73 \pm 1.00	3.1	7.55	45.81 \pm 0.83	3.50	9.62
Ta/SS316SVM	51.22 \pm 0.84	2.04	3.27	49.61 \pm 0.70	2.30	4.15
Ta/TaN/SS316SVM	48.65 \pm 0.93	5.3	22.06	36.57 \pm 0.98	5.80	26.42

The contact angle is fundamental for the characterization of the hydrophilicity characteristics of the surface, wetting, and biocompatibility properties of materials. Equation (1) is the expression that links the contact angle of a liquid on a solid with the surface tension of the solid (γ_S), the liquid (γ_L), and the solid–liquid interface ($\gamma_{S/L}$) [5]. The work of adhesion (W_a) was determined from Equation (2).

$$\cos \theta = \frac{\gamma_S - \gamma_{S/L}}{\gamma_L} \quad (1)$$

$$W_a = \gamma L - 1 - \cos \theta \quad (2)$$

The work of adhesion provides information of the work required to separate two surfaces, and from this we can obtain some information about how the hydroxyapatite coating may adhere to the surface. From Table 1, we can observe that Ti, Ta/Ti, Ta/TaN/Ti, and Ta/TaN/SS316SVM have the highest work of adhesion.

2.2. Immersion of Substrates in SBF in the Presence of Magnetic Fields

For the immersion of the substrates in simulated body fluid, a solution of 1.5 SBF was prepared according to Kokubo and Takadama [11,12]. Before immersion, the samples were washed with alcohol, placed in an ultrasound bath for 5 min, dried with compressed air, and weighed. The substrates were then immersed in SBF for 7, 10, and 14 days in a volume of simulated body fluid that was calculated using Equation (3) while maintaining a pH of 7.2–7.4 at 37 °C [12], and magnetic fields in the range 0.15 and 0.22 T were applied. These magnetic fields were generated using neodymium magnets of $40 \times 30 \times 10 \text{ mm}^3$, as shown in Figure 1. Additionally, a simulation of the field decay with distance was carried out in order to determine the uniformity of the magnetic field over the distance between the substrates and magnets. Finite Element Method Magnetics software was used to simulate the field strength between 0.1 and 0.5 T of permanent magnets over distances from 0.1 to 10 mm. Figure 1 shows the distribution of the magnetic field over this distance; it can be observed that the applied field is uniform over the distances studied.

$$V_s = \frac{S_a}{10} \quad (3)$$

where V_s is the volume of the simulated body fluid solution in mL and S_a is the surface area of the substrate in mm^2 .

Before and after immersion for the different periods and in the presence and absence of the magnetic field, the samples were weighed using a BA-E series analytical balance with a precision of 0.0001 g.

2.3. Characterization of the HAp Film Deposition

Following the immersion time of 7, 10, and 14 days, at least five substrates from each sample were washed with distilled water, dried with compressed air, and weighed. The evaluation of the formation of HAp films was carried out using scanning electron microscopy (SEM), EDS elemental analysis, and Fourier-transform infrared spectroscopy—attenuated total reflectance (FTIR-ATR), the later using a PerkinElmer Spectrum 100 spectrophotometer and a wavenumber range of $4000\text{--}5000 \text{ cm}^{-1}$. In addition, hydrophilicity tests were carried out on the substrates that showed better formation of HAp films.

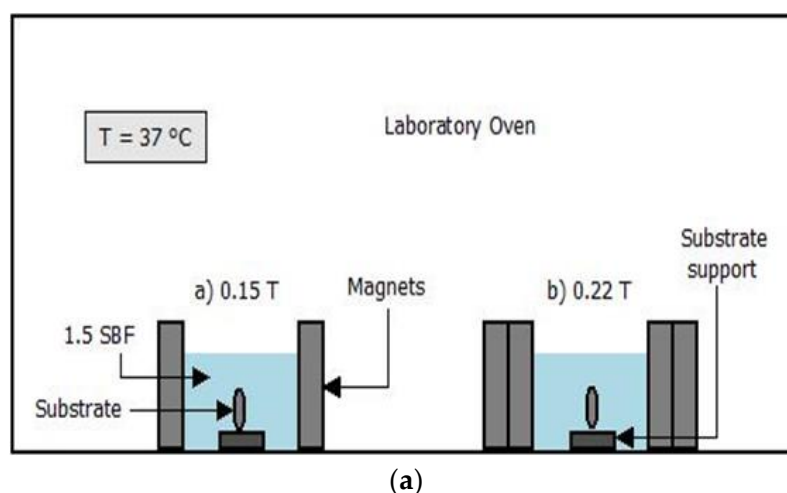
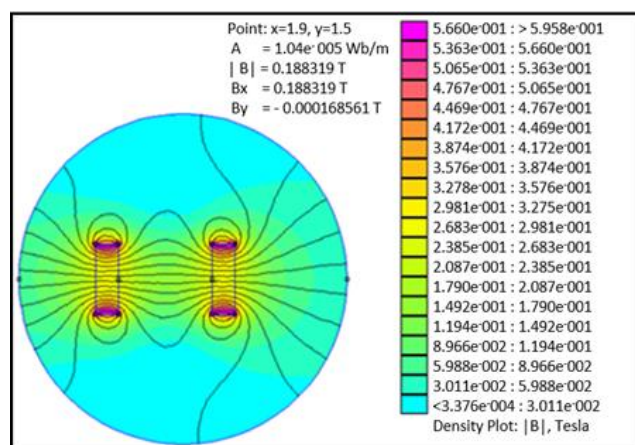


Figure 1. Cont.



(b)

Figure 1. (a) Scheme of the immersion of the substrate in simulated body fluid in the presence of magnetic fields of 0.15 T and 0.22 T. (b) Simulation of the magnetic field distribution with separation distance of magnets.

3. Results and Discussion

The SEM images of the surface-modified Ti and SS316LVM substrates are shown in Figures 2 and 3. For the polished titanium substrate (Figure 2a), a smooth morphology without a grain microstructure was obtained. After chemical treatment, an oxide layer was formed on the surface of the titanium, which presented a morphology of a cellular microstructure (Figure 2b). As previously reported by Nouri et al. [31], the layer formed on titanium after treatment with alkali could be a type of sodium titanate produced by the reaction of the former with TiO_2 . The formation of this layer improves the adsorption of proteins and calcium and phosphate ions on the surface of the substrate.

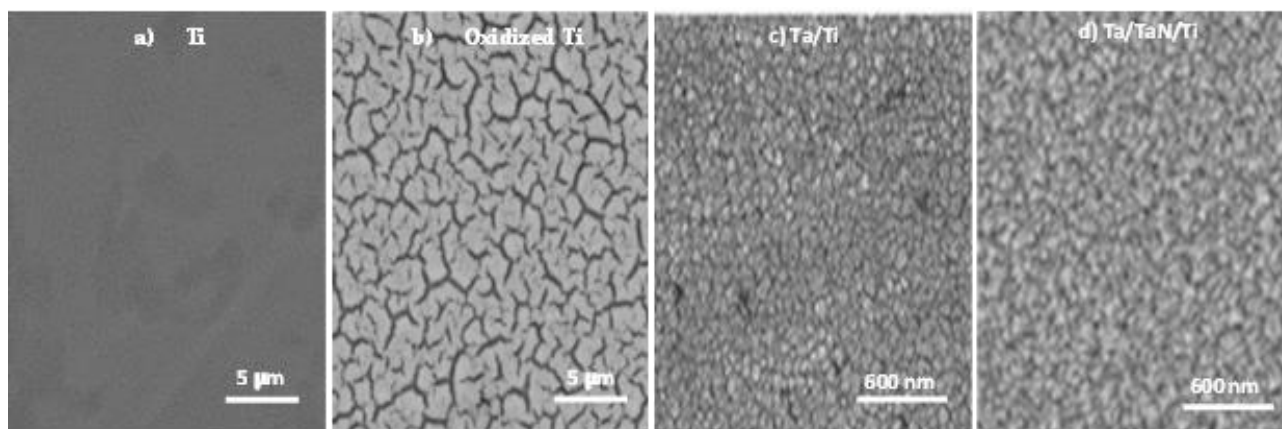


Figure 2. SEM images of the titanium substrate: (a) polished, (b) chemical treatment, (c) with Ta layers and (d) with Ta/TaN layers. Reprinted with permission from [28] 2017 Elsevier.

Figure 3a shows a sample of SS316LVM, with an irregular topography due to the grinding process carried out with P600 grade SiC paper, producing a rough morphology on the titanium surface. This process favors the adhesion of Hap layers that will be deposited later [32]. As observed in Figure 3b, the alkaline treatment had a different effect on the steel compared with titanium, due to the resistance of SS316LVM to this treatment. Nevertheless, a sodium chromate layer could be formed after reaction with NaOH, which favors the formation of calcium phosphates on the surface [33].

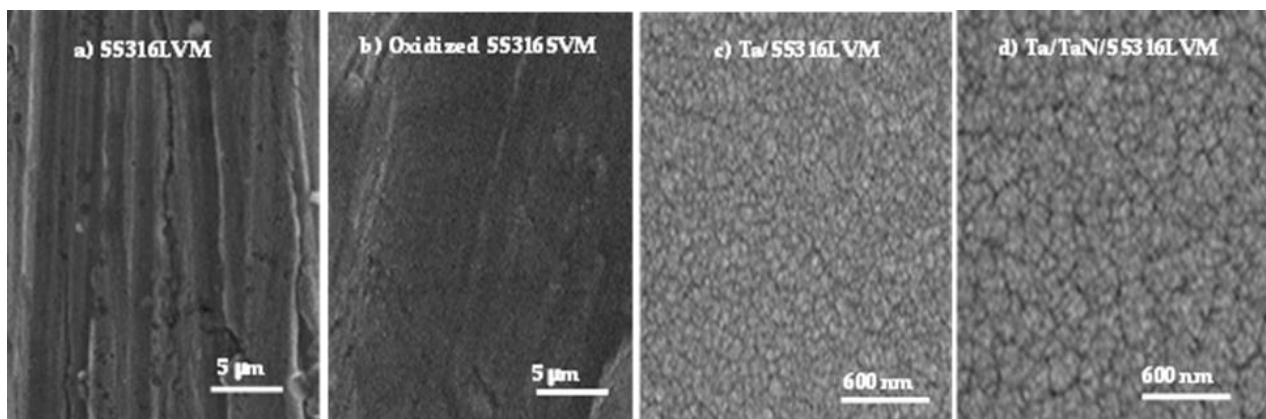


Figure 3. SEM images of the SS316LVM stainless steel substrate: (a) grinded, (b) after chemical treatment with NaOH, (c) Ta on SS316LVM, and (d) Ta/TaN on SS316LVM. Reprinted with permission from [28] 2017 Elsevier.

In contrast, Figures 2c and 3c show the deposition of the tantalum layer on Ti and on SS316LVM, respectively, with a column-like growth previously reported by Jara et al. [28]. The grain size of the Ta layer on Ti was slightly larger (60 nm) than the layer formed on the steel's surface (50 nm). Finally, Figures 2d and 3d show the deposition of Ta/TaN bilayers on Ti and SS316LVM; this double layer formed on the titanium surface was denser than the one formed on the SS316LVM.

Analysis of the Ti and SS316LVM bare materials and of the Ta and TaN coatings over the different substrates by wide-angle and grazing-angle XRD, previously reported by Jara et al. [28], showed that uncoated titanium is formed in two different crystalline structures: a cubic and a hexagonal phase. This analysis also showed the presence of TiO_2 . In contrast, grazing-angle XRD Ta/Ti and Ta/TaN/Ti showed the presence of nano- β -tantalum, as evidenced in the SEM images shown in Figure 2a,b. For the uncoated SS316LVM sample, a mixture between the two austenitic phases of steel, gamma (γ) and alpha (α), was observed. In contrast, the Ta/SS316LVM and Ta/TaN/SS316LVM showed the presence of γ -steel and α -tantalum.

3.1. Microstructure of the Hydroxyapatite Films

Figure 4 shows the SEM images of the effect of the magnetic field on the deposition of HAp on the oxidized Ti and SS316LVM substrates after 10 days of immersion in SBF. As observed in Figure 4b, a denser layer of HAp with agglomerations on the surface was formed on the oxidized Ti substrate in the presence of SBF under a magnetic field of 0.22 T compared to the substrate without the presence of a magnetic field (Figure 4a). This result is also in agreement with the obtained mass of HAp, higher mass of HAp (0.030 mg/mm^2) was obtained on Ti substrates immersed in SBF under the application of a magnetic field compared with the sample without the presence of a magnetic field (0.011 mg/mm^2 HAp). Additionally, the Ca/P ratio was 1.69, as shown in Figure 4e near the stoichiometric HAp 1.69 Ca/P ratio [8,31,32].

Both SS316LVM and Ti substrates showed similar behaviors under the presence of a magnetic field of 0.22 T: For the SS316LVM substrate, an increase in the deposition of HAp was also observed with the application of a magnetic field (Figure 4d) when compared with the sample without a magnetic field (Figure 4c); the obtained HAp mass was 0.108 mg/mm^2 , which is 18 times higher than the mass of HAp formed in the sample without the presence of a magnetic field. The morphology of the HAp layer formed on the surface of SS316LVM and on Ti is similar to the typical morphology reported for HAp. The roughness of SS316LVM increases the deposition and agglomeration of particles on the surface, due to the higher surface energy and also the topography characteristics [32]. Finally, as shown in Figure 4f, the elemental analysis of the Ca/P ratio equal to 1.39 indicated the

formation of calcium phosphate precursors of HAp on the surface and therefore suggested that Ti promotes the formation of calcium phosphate precursors of HAp at early stages [22].

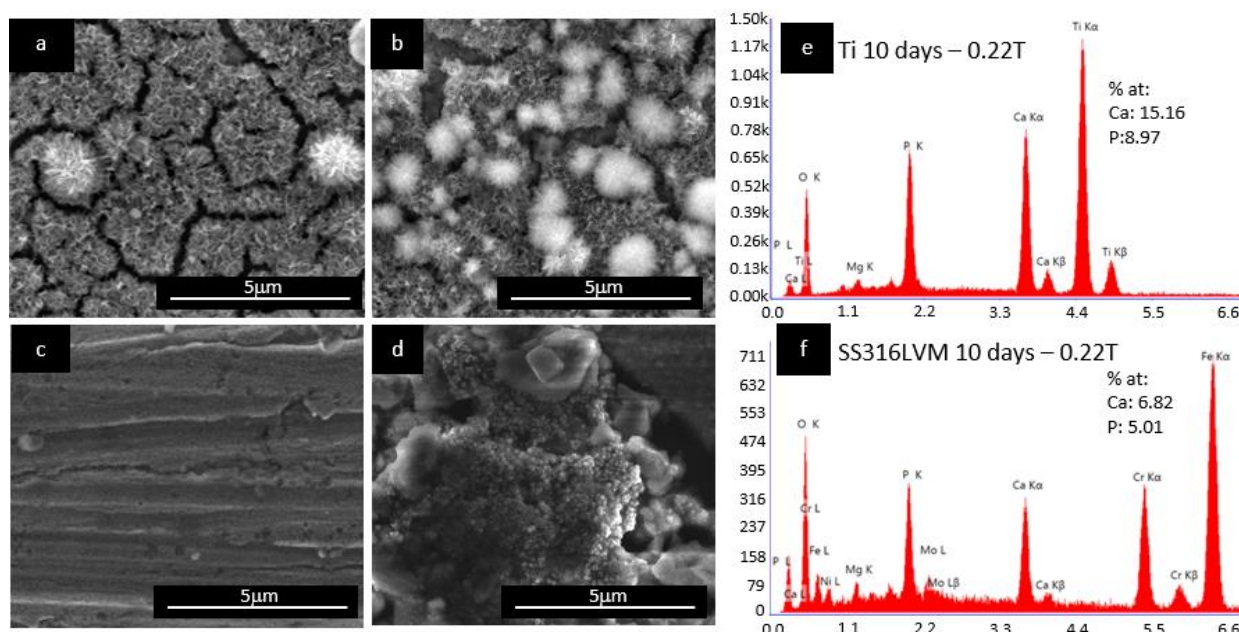


Figure 4. Deposition of HAp after immersion during 10 days in SBF: (a) Ti substrates without a magnetic field applied; (b) Ti substrates in the presence of a magnetic field of 0.22 T; (c) SS316LVM substrates without a magnetic field; (d) SS316LVM substrates in the presence of a magnetic field of 0.22 T; (e) EDS Ti, 10 days—0.22 T; and (f) EDS SS316 LVM, 10 days—0.22 T.

Figure 5 shows the influence of the SBF immersion time of the Ti substrate on the nucleation and formation of the HAp layer in the presence of a magnetic field of 0.15 T. Figure 5a shows the results after 7 days of immersion compared with 14 days of immersion (Figure 5b); a lower deposition on the Ti substrate was obtained (Ca/P ratio of 1.63, as shown in Figure 5e). Moreover, the obtained mass of HAp in the sample with 14 days of immersion was roughly six times larger (0.025 mg/mm^2 , Figure 6). Additionally, the SS316LVM substrate showed the same mass increment than the Ti substrate (Figure 5c,d) from 0.002 to 0.020 mg/mm^2 when the magnetic field exposure time was increased. In addition, the obtained Ca/P ratio of 1.20 (Figure 5f) is indicative of the possible formation of a calcium phosphate precursor of HAp [22].

The presence of a magnetic field enhanced the nucleation and growth of the HAp layer on both substrates; this effect was more pronounced at a higher magnetic field (0.22 T). Tian et al. [25] reported that the only property affected by the presence of a magnetic field in calcium phosphate precipitation is proton spinning (the proton spin is $I = 1/2$). They supposed that if the proton can leave the phosphate ion with only one of the possible spin orientations, a doubling of the transference velocity when in the presence of a sufficiently strong magnetic field can be expected. Then, the nucleation and growth rates should also be doubled in a similar fashion, as long as such rates are proportional to the proton transfer rate.

3.2. Effect of the Deposition of HAp on Ta and Ta/TaN-Covered Ti and SS316LVM Substrates

As can be seen in Figure 7a,b, the deposition of HAp on Ta/Ti and Ta/TaN/Ti was uniform, showing a coral-like morphology, which is characteristic of biomimetic formation of HAp [2,31]. For the Ta/TaN/Ti substrate, a Ca/P ratio of 1.66 (Figure 7e) was determined by EDS. When compared with the HAp layer obtained for the uncoated substrates, the Ta- and Ta/TaN-coated substrates that were kept under immersion for 14 days and were irradiated with a magnetic field of 0.22 T showed greater formation of HAp. According to Jara et al. [28], the greater formation of HAp on Ta is due to the high bioactive properties

of the latter. The deposition mechanism of HAp on tantalum follows a similar process than on Ti. It begins with the formation of Ta-OH groups on the Ta surface due to the hydration of the tantalum oxide layer that is formed during immersion in SBF. Then, Ta-OH reacts with Ca^{2+} ions, yielding a species of calcium tantalate. Next, this chemical species is combined with phosphate ions to begin heterogeneous nucleation, with the formation of an amorphous phase of calcium phosphate. Finally, excess Ca^{2+} and PO_4^{-3} ions are absorbed in the surface and rapidly form HAp.

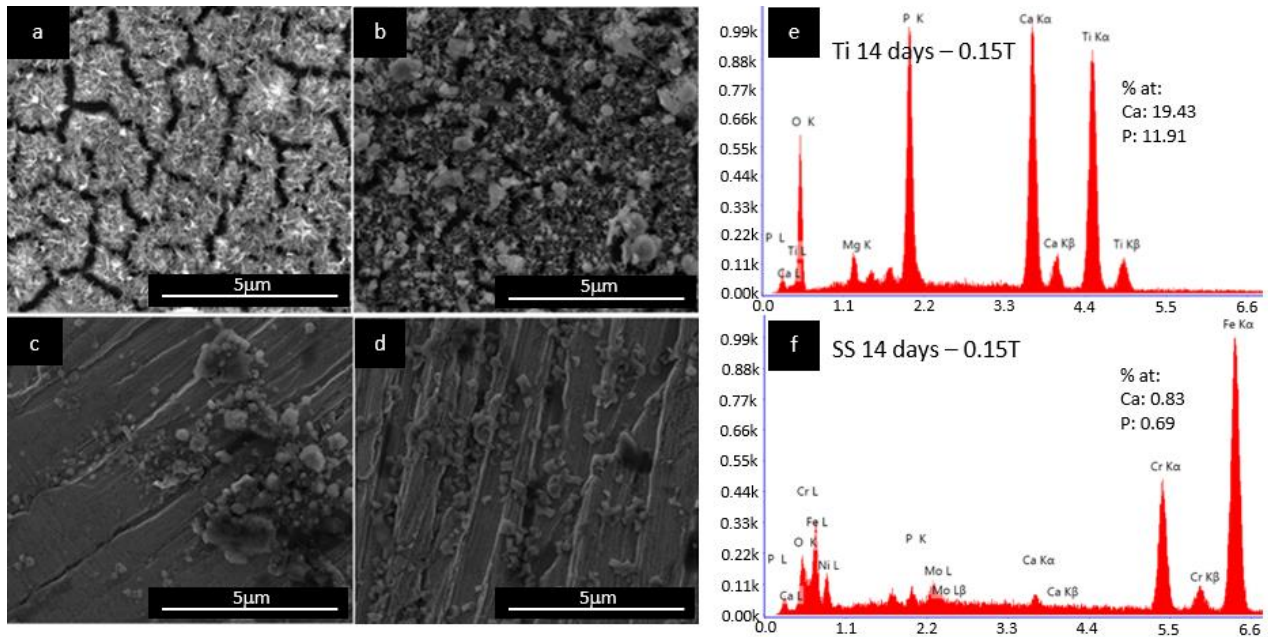


Figure 5. Deposition of HAp in (a) Ti substrates after 7 days of immersion in SBF, in the presence of a magnetic field of 0.15 T; (b) Ti substrates after 14 days of immersion in SBF, in the presence of a magnetic field of 0.15 T; (c) SS substrates after 10 days of immersion in SBF, in the presence of a magnetic field of 0.15 T; (d) SS substrates after 14 days of immersion in SBF, irradiated with a magnetic field of 0.15 T; (e) EDS Ti, 14 days—0.15 T; and (f) EDS SS, 14 days—0.15 T.

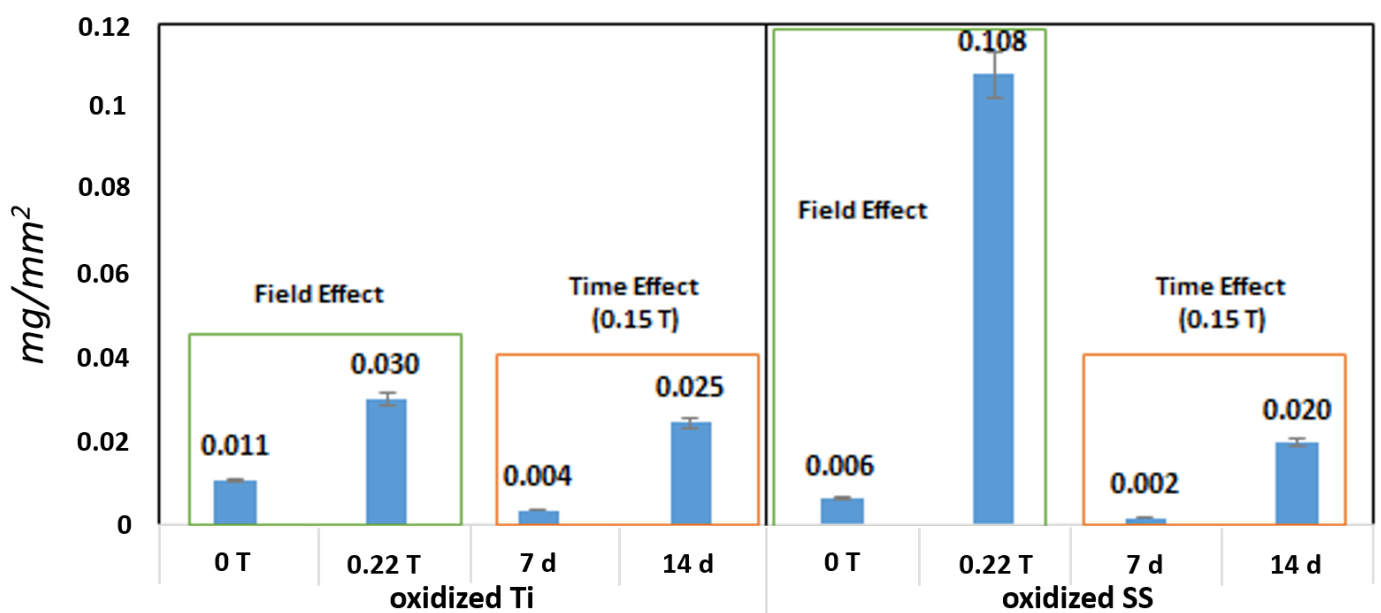


Figure 6. Mass of HAp obtained on Ti and SS substrates under different magnetic field conditions and exposure times.

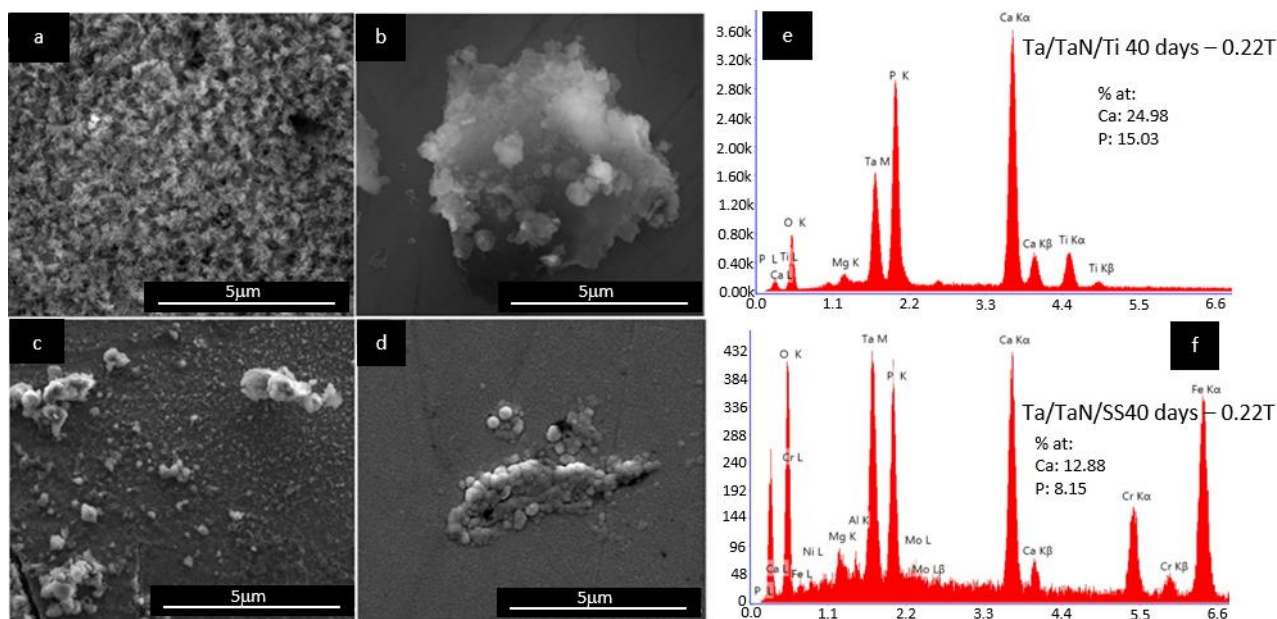


Figure 7. Deposition of HAP at 14 days and 0.22 T on (a) Ta/TaN/Ti, (b) Ta/Ti, (c) Ta/SS, (d) Ta/TaN/SS, (e) Ta/TaN/Ti EDS, and (f) Ta/TaN/SS EDS.

When analyzing Ta/SS and Ta/TaN/SS materials (Figure 7c,d), we observed a fine, uniform deposition layer of HAP and the formation of some agglomerates with a Ca/P ratio of 1.6 (Figure 7f). In contrast, the Ta/SS substrate did not show satisfactory deposition of HAP when in the presence of a magnetic field of 0.22 T; rather, the sample only presented an initial precipitation phase of HAP on the substrate. This negative effect can be attributed to the delamination of the Ta layer on the steel substrate [28]. Moreover, the Ta/SS substrate showed less formation of HAP ($<0.001 \text{ mg/mm}^2$) when compared to the HAP deposition masses on the rest of the substrates after irradiation with 0.22 T (Figure 8).

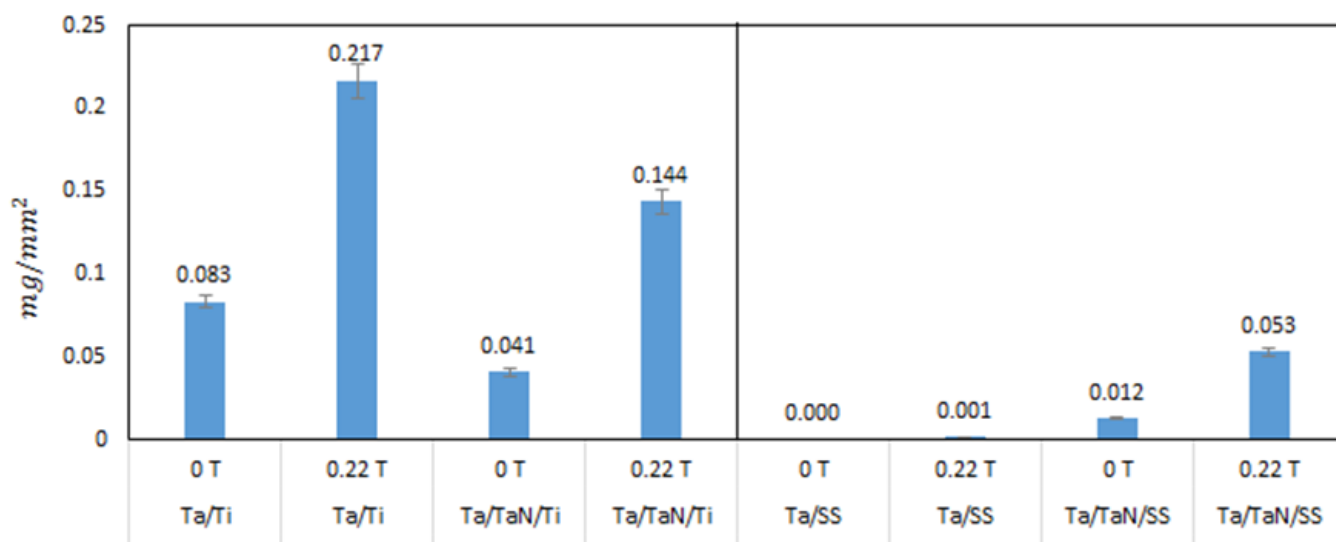


Figure 8. Mass of HAP formed on Ta- and Ta/TaN-covered Ti and SS substrates after 14 days.

3.3. FTIR Spectra Results

Figure 9 shows the FTIR spectra of the deposition of the different substrates in a range 700 to 2000 cm^{-1} . As shown in Figure 9a, the Ti substrate in the presence of a magnetic field yielded show an increase in the intensity of PO_4^{3-} vibration ($1110\text{--}1020 \text{ cm}^{-1}$) and

the OH^- (1630 cm^{-1}) group present in calcium phosphates. In contrast, the deposition on titanium showed the typical bands of calcium phosphate and an additional symmetric vibration of the phosphate at 960 cm^{-1} [34] after immersion up to 14 days. In addition, when analyzing the Ta/Ti substrate, a more defined band at $1110\text{--}1020\text{ cm}^{-1}$ could be observed as evidence of the formation of the HAp phase on the substrate.

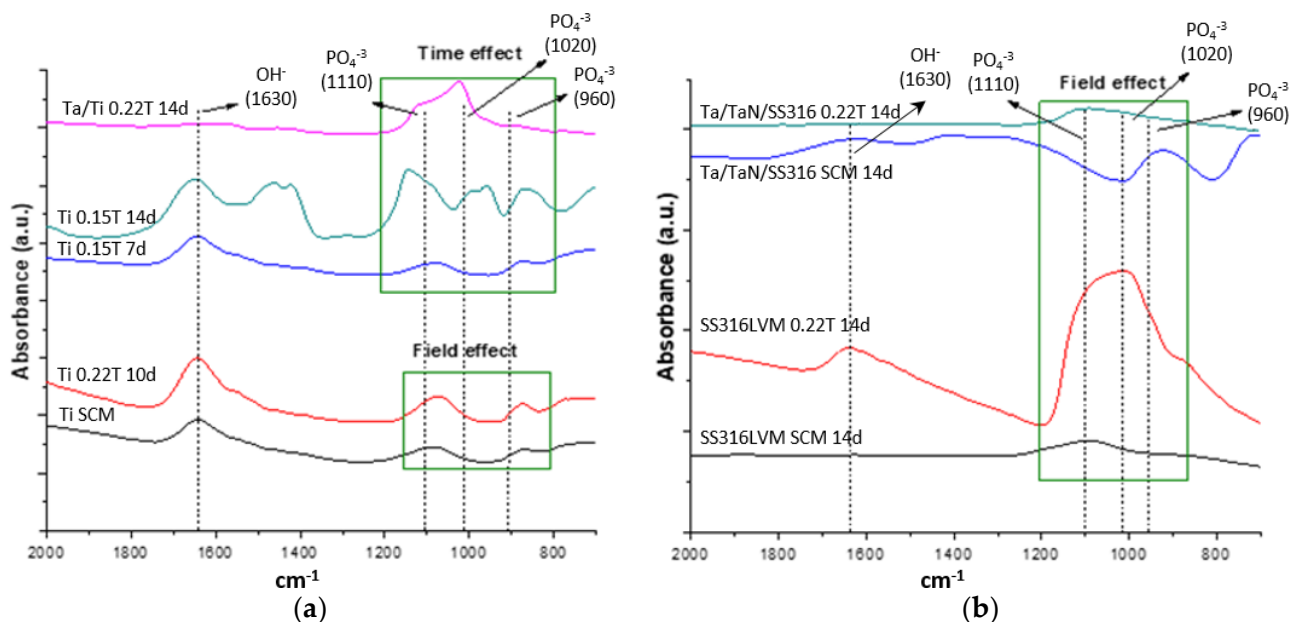


Figure 9. FTIR spectra of HAp deposition at different magnetic fields and immersion times on Ti (a) and SS316LVM (b) substrates.

In a similar trend, Figure 9b shows a defined spectrum on the deposition layer on the SS316LVM substrate in the presence of a magnetic field. For the Ta/SS substrate, the spectrum does not show the characteristic bands corresponding to calcium phosphate, which is in agreement with the previously discussed SEM results. Finally, the Ta/TaN/SS substrate (Figure 9b) showed a band at $1110\text{--}1020\text{ cm}^{-1}$, which is indicative of a phosphate group.

3.4. Contact Angle Measurements

The data shown in Table 2 correspond to the results of the surface test carried out using a contact angle measurement before and after the deposition of HAp on the substrates that yielded a higher mass of HAp. The chemically treated titanium substrate (before deposition) showed an angle of $67.08 \pm 0.63^\circ$, which is in agreement with reports for Ti after acid treatment [35]. The obtained angle lies within the range for a hydrophilic surface ($10^\circ < \theta < 90^\circ$) [36], and this hydrophilicity characteristic is higher in materials with coatings of Ta and Ta/TaN, which presented contact angles of $48.52 \pm 0.91^\circ$ and $46.22 \pm 0.66^\circ$ (respectively), in good agreement with the other reports [37]; this behavior is desirable for cell adhesion. If the surface is hydrophobic, the adhesion between the cell culture and the implant will be poor [38]. After the deposition of HAp, a decrease in the contact angle could be observed for all the samples, indicating a high hydrophilic property desirable in a biocompatible material.

For the SS316LVM sample, a contact angle of $46.73 \pm 1.00^\circ$ was measured before the deposition of HAp. Nevertheless, with coatings of Ta/TaN and Ta layers, the magnitudes of the contact angles obtained ($48.65 \pm 0.93^\circ$ and $51.22 \pm 0.84^\circ$) slightly increase [28]. For the polished SS316LVM sample, the reported contact angle was 63.33° [39], which shows that both the chemical treatment and the deposition with Ta and Ta/TaN layers improve the hydrophilicity of the substrate. After the deposition of HAp, the contact angle decreased mainly for Ta/TaN/SS, due to the beneficial effect of this coating for their application as biomaterials. Table 2 also shows the work of adhesion; this is the work required to

separate two phases in contact at the interface. We calculated this from Equation (2). We observed that higher values were obtained for Ti, Ta/Ti, Ta/SS316SVM, and Ta/TaN/SS316SVM, indicating the beneficial effect of these coatings, especially on steel, improving the adherence to HAp, and also protecting the material against corrosion, preventing Fe and Cr ions to be release into body fluids.

Table 2. Contact angle in different substrates with the obtained higher mass of HAp.

Substrate	Bare Substrate	After HAp Deposition	Work of Adhesion
	Angle (°)	Angle (°)	Wa (mJ/m ²)
Ti	67.08 ± 0.63	44.15 ± 0.99	142.99
Ta/Ti	48.52 ± 0.91	44.88 ± 0.70	116.89
Ta/TaN/Ti	46.22 ± 0.66	35.80 ± 0.63	48.78
SS316SVM	46.73 ± 1.00	45.81 ± 0.83	53.71
Ta/SS316SVM	51.22 ± 0.84	49.61 ± 0.70	129.08
Ta/TaN/SS316SVM	48.65 ± 0.93	36.57 ± 0.98	102.78

4. Conclusions

The metallic titanium and BIOLINE SS316LVM substrates showed surface formation of oxides after chemical treatment during biomineralization, which favors the deposition of HAp under the action of a magnetic field of 0.22 T. Under these conditions, the SS316LVM substrate presented the most favorable deposition of HAp (0.108 mg/mm²). In addition, the HAp deposits on both Ti and SS316LVM substrates showed a characteristic morphology with Ca/P ratios of 1.69 and 1.63, respectively, which is characteristic of non-stoichiometric HAp. The surface modifications of the titanium surface with Ta and Ta/TaN enhanced the bioactivity of the substrates; this is consistent with the values of work of adhesion obtained for these substrates

It was shown that the application of magnetic fields following the biomimetic method had a significant effect on the formation of HAp on the different substrates studied (immersed in simulated body fluid for 14 days and irradiation of 0.22 T) by increasing the obtained mass/area ratio of HAp by 55.36% on average when compared with the biomimetic traditional method. Nevertheless, modifications of the SS316LVM substrate with Ta and Ta/N yielded a positive effect of the magnetic field on HAp deposition. Measuring the contact angle before and after the HAp deposition proved the hydrophilic behavior of Ti and SS316LVM substrates, as desired for biomaterial applications. These materials are promising for in vivo therapeutic applications in the presence of a magnetic field shortening the period of bone regeneration.

Author Contributions: Conceptualization, R.U. and G.G.; methodology, R.U., A.U., O.B., L.L. and G.G.; validation, R.U., O.B. and G.G.; formal analysis, A.U., R.U. and G.G.; investigation, R.U., A.U., O.B., L.L. and G.G.; resources, O.B. and R.U.; data curation, R.U., L.L. and G.G.; writing—original draft preparation, A.U. and R.U.; writing—review and editing, R.U. and G.G.; visualization, R.U., A.U., O.B., L.L. and G.G.; supervision, R.U., O.B., L.L. and G.G.; project administration, O.B. and R.U.; funding acquisition, O.B. and R.U. All authors have read and agreed to the published version of the manuscript.

Funding: This research was funded by the project EPN-PIMI 17-05, “Desarrollo de sistemas de hidroxiapatita dopados con óxidos metálicos biocompatibles para aplicaciones biomédicas,” Escuela Politécnica Nacional, Quito-Ecuador.

Institutional Review Board Statement: Not applicable.

Informed Consent Statement: Not applicable.

Data Availability Statement: Not applicable.

Acknowledgments: The authors would like to thank the Vicerrectorado de Investigación, Innovación y Vinculación, Escuela Politécnica Nacional, and the Universidad Yachay Tech del Ecuador.

Conflicts of Interest: The authors declare no conflict of interest.

References

1. Javaid, M.A.; Kaartinen, M.T. Mesenchymal Stem Cell-based Bone Tissue Engineering. *Int. Dent. J. Stud. Res.* **2013**, *1*, 24–35.
2. Baker, K.C.; Anderson, M.A.; Oehlke, S.A.; Astashkina, A.I.; Haikio, D.C.; Drelich, J.; Donahue, S.W. Growth, Characterization and Biocompatibility of Bone-like Calcium Phosphate Layers Biomimetically Deposited on Metallic Substrata. *Mater. Sci. Eng. C* **2006**, *26*, 1351–1360. [[CrossRef](#)]
3. Surmeneva, M.; Vladescu, A.; Surmenev, R.; Pantilimon, C.; Braic, M.; Cotrut, C. Study on a hydrophobic Ti-doped hydroxyapatite coating for corrosion protection of a titanium-based alloy. *RSC Adv.* **2016**, *6*, 87665–87674. [[CrossRef](#)]
4. Bauer, S.; Schmuki, P.; Mark, K.; Park, J. Engineering biocompatible implant surfaces: Part I: Materials and surfaces. *Prog. Mater. Sci.* **2013**, *58*, 261–326. [[CrossRef](#)]
5. Flores-Fraile, J.; Ramírez, J.M.; Macedo de Sousa, B.; Herrero-Hernández, S.; López-Valverde, A. Bioactive Surfaces vs. Conventional Surfaces in Titanium Dental Implants: A Comparative Systematic Review. *J. Clin. Med.* **2020**, *9*, 2047. [[CrossRef](#)]
6. Thirugnanam, A.; Sampath, T.S.; Chakkingal, U. Bioactivity Enhancement of Commercial Pure Titanium by Chemical Treatments. *Trends Biomater. Artif. Organs.* **2009**, *23*, 76–85.
7. Szcześ, A.; Hołysz, L.; Chibowski, E. Synthesis of Hydroxyapatite for Biomedical Applications. *Adv. Colloid Interface Sci.* **2017**, *249*, 321–330. [[CrossRef](#)]
8. Chetty, A.; Wepener, I.; Marei, M.K.; El Kamary, Y.; Moussa, R.M. *Hydroxyapatite: Synthesis, Properties and Applications*; Nova Science Publishers: Hauppauge, NY, USA, 2012; pp. 91–132.
9. Al-Amin, M.; Abdul-Rani, A.M.; Danish, M.; Rubaiee, S.; Mahfouz, A.B.; Thompson, H.M.; Ali, S.; Unune, D.R.; Sulaiman, M.H. Investigation of Coatings, Corrosion and Wear Characteristics of Machined Biomaterials through Hydroxyapatite Mixed-EDM Process: A Review. *Materials* **2021**, *14*, 3597. [[CrossRef](#)] [[PubMed](#)]
10. Gil, J.; Manero, J.M.; Ruperez, E.; Velasco-Ortega, E.; Jiménez-Guerra, A.; Ortiz-García, I.; Monsalve-Guil, L. Mineralization of Titanium Surfaces: Biomimetic Implants. *Materials* **2021**, *14*, 2879. [[CrossRef](#)]
11. Kokubo, T.; Kim, H.M.; Kawashita, M. Novel Bioactive Materials with Different Mechanical Properties. *Biomaterials* **2003**, *24*, 2161–2175. [[CrossRef](#)]
12. Kokubo, T.; Takadama, H. How Useful is SBF in Predicting in Vivo Bone Bioactivity? *Biomaterials* **2006**, *27*, 2907–2915. [[CrossRef](#)]
13. Lindahl, C. Biomimetic Deposition of Hydroxyapatite on Titanium Implant Materials. Ph.D. Thesis, Universidad de Uppsala, Uppsala, Sweden, 2012.
14. Pecheva, E.; Pramatarova, L.; Maitz, M.F.; Pham, M.T. Study of the Calcium Phosphate Layer Grown on AISI 316 Stainless Steel from a Simulated Body Fluid. *J. Mater. Sci. Mater. Electron.* **2003**, *14*, 775–776. [[CrossRef](#)]
15. Nicolas-Silvente, A.I.; Velasco-Ortega, E.; Ortiz-García, I.; Monsalve-Guil, L.; Gil, J.; Jiménez-Guerra, A. Influence of the titanium implant surface treatment on the surface roughness and chemical composition. *Materials* **2020**, *13*, 314. [[CrossRef](#)] [[PubMed](#)]
16. Petrović, Ž.; Katić, J.; Šarić, A.; Despotović, I.; Matijaković, N.; Leskovic, M.; Kralj, D.; Petković, M. Influence of Biocompatible Coating on Titanium Surface Characteristics. *Innov. Corros. Mater. Sci.* **2020**, *10*, 37–46. [[CrossRef](#)]
17. Levine, B.R.; Sporer, S.; Poggio, R.A.; Della Valle, C.J.; Jacobs, J.J. Experimental and clinical performance of porous tantalum in orthopedic surgery. *Biomaterials* **2006**, *27*, 4671–4681. [[CrossRef](#)] [[PubMed](#)]
18. Leng, Y.X.; Sun, H.; Yang, P.; Chen, J.Y.; Wang, J.; Wan, G.J.; Chu, P.K. Biomedical properties of tantalum nitride films synthesized by reactive magnetron sputtering. *Thin Solid Film.* **2001**, *398*, 471–475. [[CrossRef](#)]
19. Matsuno, H.; Yokoyama, A.; Watari, F.; Uo, M.; Kawasaki, T. Biocompatibility and osteogenesis of refractory metal implants, titanium, hafnium, niobium, tantalum and rhenium. *Biomaterials* **2001**, *22*, 1253–1262. [[CrossRef](#)]
20. Maccauro, G.; Iommetti, P.R.; Muratori, F.; Raffaelli, L.; Manicone, P.F.; Fabbriani, C. An overview about biomedical applications of micron and nano size tantalum. *Recent Pat. Biotechnol.* **2009**, *3*, 157–165. [[CrossRef](#)]
21. Koutsopoulos, S. Synthesis and Characterization of Hydroxyapatite Crystals: A Review Study on the Analytical Methods. *J. Biomed. Mater. Res.* **2002**, *62*, 600–612. [[CrossRef](#)] [[PubMed](#)]
22. Drouet, C. Apatite Formation: Why It May Not Work as Planned, and How to Conclusively Identify Apatite Compounds. Open Archive Toulouse Archive Ouverte (OATAO). *BioMed Res. Int.* **2013**, *2013*, 1–12. [[CrossRef](#)]
23. Sorensen, J.S.; Lundager, H.E. Influence of Magnetism on Precipitation of Calcium Phosphate. *J. Cryst. Growth* **2000**, *216*, 399–406. [[CrossRef](#)]
24. Sequeda, L.G.; Díaz, J.M.; Gutiérrez, S.J.; Perdomo, S.J.; Gómez, O.L. Synthetic hydroxyapatite obtaining using three different methods and characterization to use it as bone substitute. *Rev. Colomb. de Cienc. Químico-Farm.* **2012**, *41*, 50–66.
25. Tian, A.; Xue, X.; Liu, C.; He, J.; Yang, Z. Electrodeposited Hydroxyapatite Coatings in Static Magnetic Field. *Mater. Lett.* **2010**, *64*, 1197–1199. [[CrossRef](#)]
26. Sundaram, N.M.; Giriya, E.K.; Ashok, M.; Anee, T.K.; Vani, R.; Suganthi, R.V.; Yokogawa, Y.; Kalkura, S.N. Crystallisation of Hydroxyapatite Nanocrystals Under Magnetic Field. *Mater. Lett.* **2006**, *60*, 761–765. [[CrossRef](#)]
27. Siddharthan, A.; Sampath, T.S.; Seshadri, S.K. Effect of Magnetic Field on Biomimetic Coating of Hydroxyapatite on Titanium. *Trends Biomater. Artif. Organs* **2006**, *20*, 12–15.

28. Jara, A.; Fraisse, B.; Flaud, V.; Fréty, N.; Gonzalez, G. Thin Film Deposition of Ta, TaN and Ta/TaN Bi-Layer on Ti and SS316-LVM Substrates by RF sputtering. *Surf. Coat. Technol.* **2017**, *309*, 887–896. [[CrossRef](#)]
29. ASTM International. *ASTM E3-11 (2017): Standard Practice for Preparation of Metallographic Specimens*; ASTM International: West Conshohocken, PA, USA, 2017.
30. Burgués, J.T. *Medida del Ángulo de Contacto*; Technical Report; Departamento de Ingeniería Química EPN: Quito, Ecuador, 2013; pp. 1–62.
31. Nouri, A.; Hodgson, P.D.; We, C. Biomimetic Porous Titanium Scaffolds for Orthopedic and Dental Applications. In *Biomimetics Learning from Nature*; Mukherjee, A., Ed.; InTech: London, UK, 2010. [[CrossRef](#)]
32. Kadhim, M.; Abdulateef, N.; Abdulkareem, M. Evaluation of Surface Roughness of 316L Stainless Steel Substrate on Nanohydroxyapatite by Electrophoretic Deposition. *Al-Nahrain J. Eng. Sci.* **2018**, *21*, 28–35. [[CrossRef](#)]
33. Huynh, V.; Ngo, N.; Golden, T. Surface Activation and Pretreatments for Biocompatible Metals and Alloys Used in Biomedical Applications. *Int. J. Biomater.* **2019**, *2019*, 3806504. [[CrossRef](#)]
34. Cimdina, L.B.; Borodajenko, N. Research of Calcium Phosphates Using Fourier Transform Infrared Spectroscopy. In *Infrared Spectroscopy*; Theophile, P.T., Ed.; InTech: London, UK, 2012; pp. 124–148.
35. Strnad, G.; Chirila, N.; Petrovan, C.; Russu, O. Contact Angle Measurement on Medical Implant Titanium-based Biomaterials. *Procedia Technol.* **2016**, *22*, 946–953. [[CrossRef](#)]
36. Minagar, S.; Berndt, C.C.; Wen, C. Fabrication and Characterization of Nanoporous Niobia, and Nanotubular Tantalum, Titania and Zirconia via Anodization. *J. Funct. Biomater.* **2015**, *6*, 153–170. [[CrossRef](#)]
37. Balla, V.K.; Banerjee, S.; Bose, S.; Bandyopadhyay, A. Direct Laser Processing of a Tantalum Coating on Titanium for Bone Replacement Structures. *Acta Biomater.* **2010**, *6*, 2329–2334. [[CrossRef](#)] [[PubMed](#)]
38. Menzies, K.L.; Jones, L. The Impact of Contact Angle on the Biocompatibility of Biomaterials. *Optom. Vis. Sci.* **2010**, *87*, 387–399. [[CrossRef](#)] [[PubMed](#)]
39. Padhi, A.K. Surface Modification of 316L Stainless Steel by Sol-Gel Method. Ph.D. Thesis, National Institute of Technology, Patna, India, 2014.